Acta Astronautica 79 (2012) 241–252

Contents lists available at SciVerse ScienceDirect

Acta Astronautica

journal homepage: www.elsevier.com/locate/actaastro

Constant-thrust glideslope guidance algorithm for time-fixed rendezvous in real halo orbit

Yijun Lian*, Yunhe Meng, Guojian Tang, Luhua Liu

College of Aerospace and Material Engineering, National University of Defense Technology, Changsha 410073, China

ARTICLE INFO

Article history:
Received 7 May 2011
Received in revised form
17 March 2012
Accepted 29 April 2012
Available online 29 May 2012

Keywords:
Glideslope guidance
Rendezvous and Docking
Real halo orbit
Guidance and control
Full ephemeris model

ABSTRACT

This paper presents a fixed-time glideslope guidance algorithm that is capable of guiding the spacecraft approaching a target vehicle on a quasi-periodic halo orbit in real Earth–Moon system. To guarantee the flight time is fixed, a novel strategy for designing the parameters of the algorithm is given. Based on the numerical solution of the linearized relative dynamics of the Restricted Three-Body Problem (expressed in inertial coordinates with a time-variant nature), the proposed algorithm breaks down the whole rendezvous trajectory into several arcs. For each arc, a two-impulse transfer is employed to obtain the velocity increment (delta-v) at the joint between arcs. Here we respect the fact that instantaneous delta-v cannot be implemented by any real engine, since the thrust magnitude is always finite. To diminish its effect on the control, a thrust duration as well as a thrust direction are translated from the delta-v in the context of a constant thrust engine (the most robust type in real applications). Furthermore, the ignition and cutoff delays of the thruster are considered as well. With this high-fidelity thrust model, the relative state is then propagated to the next arc by numerical integration using a complete Solar System model. In the end, final corrective control is applied to insure the rendezvous velocity accuracy. To fully validate the proposed guidance algorithm, Monte Carlo simulation is done by incorporating the navigational error and the thrust direction error. Results show that our algorithm can effectively maintain control over the time-fixed rendezvous transfer, with satisfactory final position and velocity accuracies for the near-range guided phase.

1. Introduction

The near-earth Rendezvous and Docking (RVD) problem has been studied in depth [1–9] since the 1960s, but not too much progress has been done in the rendezvous problem in multi-body realm. However, in view of the great potentials of L1 and L2 in Earth–Moon system (such as the portal of the IPS (InterPlanetary Superhighway) [10] and space-based depot for lunar exploration [11]), the problem of libration point orbit rendezvous should be well addressed. Unlike the near-earth case, practical orbits around libration points usually have very large scales, both in time and space. One of the most frequently used families is the halo orbit. In the Circular Restricted Three-Body Problem (CRTBP), there are purely periodic halo orbits; in the full ephemeris model, only quasi-periodic halo orbits stand [12], which we will refer to as real halo orbits (or halo orbits for short) in this paper. The exact determination of halo orbits has to resort to numerical methods. Moreover, these orbits are essentially very unstable due to the high nonlinearity of the problem, posing great challenge to the guidance and control system design.

There are already some works focusing on the halo-to-halo transfers, which could be viewed as one type of halo

* Correspondence to: College of Aerospace and Material Engineering, National University of Defense Technology; Yanwachi Zheng Street No. 47, Changsha 410073, Hunan Province, China. Tel.: +8673184573140.
E-mail address: missilelyj@163.com (Y. Lian).

0094-5765/$ - see front matter © 2012 Elsevier Ltd. All rights reserved.
http://dx.doi.org/10.1016/j.actaastro.2012.04.049

orbit rendezvous. Hiday-Johnston and Howell [13–15] applied primer vector theory [16] to the transfer design between halo orbits in Elliptical Restricted Three-Body Problem (ERTBP), and found some local cost-optimal results. Gómez et al. [17] developed two methods to solve the same problem in CRTBP, based on the phase space geometry and Floquet theory, respectively. The obtained results were compared with those of Hiday-Johnston and Howell [14]. Roberts [18] introduced two impulsive strategies for halo-to-halo and halo-to-Lissajous transfers for the SOHO (Solar Heliospheric Observatory) mission. Volle [19] studied the halo transfer problem in the Sun–Earth/Moon system using optimal control theory, and finite thrust engine with variable specific impulse was assumed. In general, the aforementioned literature takes no account of either the gravitational forces other than from the primaries, or errors during the transfer (such as the navigational error and the implementation error, or control error), thus belongs to the trajectory design or mission planning topics.

The scope of this paper falls within the guidance and control problem of the real halo orbit rendezvous. Only a few works are found dealing with this subject. Jones [20] has done some pioneering work on terminal phase rendezvous in CRTBP. The targeting law proposed was in fact a two-impulse transfer scheme, which is only applicable for small amplitude halo orbits and small rendezvous ranges. Marinescu et al. [21,22] studied the minimum propellant optimal low-thrust rendezvous problem, but the target was the libration point itself, and only planar results were given. On the other hand, research on the near-earth rendezvous guidance problem is abundant, among which, Hablani et al. [23] proposed algorithms based on traditional glideslope guidance with astronauts in the loop, for spacecraft to approach, to fly around, and to depart from a target vehicle in a near-earth circular orbit. The closed-form solution of the linear Clohessy–Wiltshire (C–W) equations [1] was utilized and the algorithms were based on the impulsive assumption. The flight time in Hablani's work is a free parameter with no special attention paid to.

In view of the importance of the flight time in RVD mission (especially with man involved), the purpose of this study is to develop an algorithm for time-fixed missions to guide the spacecraft to approach a target vehicle in a real halo orbit, extending the near-earth RVD to multi-body realm. To this end, several reference frames and dynamical models are introduced in Section 2. A practical constant thrust model is given in Section 3, having considered the ignition and cutoff delays as well as a linear thrust establishing and vanishing process. The guidance algorithm is presented in Section 4, in which a new scheme for designing the control parameters for a given flight time is derived. In Section 5, impacts of these parameters on the algorithm performance are analyzed for a typical standard trajectory, followed by Monte Carlo simulations in consideration of navigation and control errors. Results have reliably justified both the effectiveness and robustness of the proposed algorithm in real applications. Appropriate conclusions are drawn in Section 6.

2. Equations of motion

Spacecraft are usually designated chaser and target in the rendezvous scenario, in which the target is intended to follow a ballistic trajectory (such as a halo orbit of interest) with infrequent orbit maintenance maneuvers. Control is only applied to the chaser to approach or depart from the target.

By referring to the near-earth case [7–9], we divide the halo orbit rendezvous into three consecutive phases: far-range guided phase, near-range guided phase, and final approach phase. In the first phase, no relative navigation is established between the two spacecraft, and the chaser uses absolute navigational means to approach the target. In the second phase, relative measuring information is available and relative motion is usually considered in the guidance methodologies. Lastly, the final approach phase will deliver the chaser to the docking position through a distance of hundreds of meters, along which path the six-degree-of-freedom (both the translational and rotational motion) control must be applied.

In this study, only the near-range guided phase is considered. In the first place, several reference frames and dynamical models are introduced as follows.

2.1. Geocentric J2000.0 coordinates frame and related dynamical model

The origin of the geocentric J2000.0 frame, designated by O_E-XYZ, is at the barycenter of the Earth. The X-axis points at the mean J2000.0 vernal equinox, and the X–Y plane coincides with the mean equatorial plane.

The equations of motion described in O_E-XYZ is given by

$$\ddot{\boldsymbol{r}} = -\frac{\mu_E}{r^3}\boldsymbol{r} + \boldsymbol{f}_M + \boldsymbol{f}_S + \boldsymbol{f}_P + \frac{F}{m}\boldsymbol{n} \tag{1}$$

where $r = \|\boldsymbol{r}\|$, $\boldsymbol{r}$ is the geocentric position vector, μ_E the earth gravitational constant (3.986004328969E14 m^3 s^{-2}), $\boldsymbol{f}_M$ the lunar gravitational acceleration, $\boldsymbol{f}_S$ the solar gravitational acceleration, $\boldsymbol{f}_P$ the sum of planetary gravitational accelerations, F the thrust magnitude, m the spacecraft mass, and $\boldsymbol{n}$ the thrust direction vector. The accelerations induced by the celestial bodies are calculated by the Newton's gravitational law, with the positions of the planets given by the JPL DE405 ephemeris. Note that this frame is not inertial; therefore, the impact of the motion of the Earth should be implicitly removed from those gravitational force items.

The equation related to mass consumption is described in [24]

$$\dot{m} = -F/c \tag{2}$$

where c is the exhaust velocity.

By numerically integrating Eqs. (1) and (2), geocentric states of the two spacecraft are obtained, from which the relative states are further calculated.

2.2. Earth–Moon L1 rotating reference of frame

Earth–Moon L1 rotating frame (or rotating frame for short), designated by $L-x_ry_rz_r$, has its origin at the geometric L1 point which is located between the two primaries. The x_r-axis is along the vector from the Earth to the Moon, and the x_ry_r plane is the instantaneous lunar orbital plane with z_r-axis as its normal unit vector.

This frame is established by using the real-time positions of the Earth and the Moon read from JPL DE405 ephemeris data. Therefore, all the irregular motions of both the Moon and the Earth are implicitly considered. The quasi-halo orbit used in Section 5 is expressed in this frame.

2.3. RVD frame and relative equations of motion

The RVD frame, designated by $o-xyz$, is chosen to have its origin at the barycenter of the target, and the three axes identical to the J2000.0 triad. For halo orbit rendezvous, much convenience with the coordinate transformation is brought about by this definition, since no angular velocity is introduced.

The linearized equations of relative motion, previously adopted in formation flying at Lagrange points [25], are employed in this work to describe the dynamics of the chaser relative to the target in inertial coordinates of RTBP, which are

$$\begin{bmatrix}\dot{\boldsymbol{x}}\\ \dot{\boldsymbol{v}}\end{bmatrix}=\begin{bmatrix}\mathbf{0} & \mathbf{I_3}\\ \boldsymbol{\Xi}(t) & \mathbf{0}\end{bmatrix}\begin{bmatrix}\boldsymbol{x}\\ \boldsymbol{v}\end{bmatrix}\triangleq\mathbf{A}(t)\begin{bmatrix}\boldsymbol{x}\\ \boldsymbol{v}\end{bmatrix} \tag{3}$$

where

$$\boldsymbol{\Xi}(t)=-(c_1+c_2)\mathbf{I_3}+3c_1\boldsymbol{e}_{1T}\boldsymbol{e}_{1T}^{\mathrm{T}}+3c_2\boldsymbol{e}_{2T}\boldsymbol{e}_{2T}^{\mathrm{T}}$$

$$c_1=\mu_1\left\|\boldsymbol{r}_{1T}(t)\right\|^{-3},c_2=\mu_2\left\|\boldsymbol{r}_{2T}(t)\right\|^{-3}$$

and μ_1 is the gravitational constant of the larger primary (3.986004328969E14 $m^3\ s^{-2}$ for the Earth), μ_2 the gravitational constant of the smaller primary (4.902800582148E12 $m^3\ s^{-2}$ for the Moon), $\boldsymbol{r}_{1T}$ the target position relative to larger primary, $\boldsymbol{r}_{2T}$ the target position relative to smaller primary, $\boldsymbol{e}_{1T}$ the unit vector of $\boldsymbol{r}_{1T}$, $\boldsymbol{e}_{2T}$ the unit vector of $\boldsymbol{r}_{2T}$, and $\boldsymbol{I_3}$ a 3×3 identity matrix.

Note that the time variation in $\boldsymbol{\Xi}$ (or $\boldsymbol{A}$) is due to the relatively slow change in the location of the target relative to the primaries. Also notice that the relative motion model (3) imposes no constraints on the type of the spacecraft orbit, which means it applies to all the orbit types in the three body problem. This model will be utilized in the proposed guidance algorithm in Section 4.

3. Constant thrust model

Engines of constant thrust are the most common and robust type in practical applications. Ideally, it has a step function thrust profile, i.e., the thrust jumps from zero to the nominal magnitude in an instant or vice versa. However, the actual situation is, although holding constant for most of the burn time, the thrust profile has, inevitably, both ignition and cutoff delays and a continuous rise-and-fall process, which is usually difficult to model accurately because the establishments of both the propellants pipe flow and the combustion gas filling are highly nonlinear. Therefore, a constraint of minimum thrust time is induced, that is, a null or insufficient magnitude will be exerted if the commanded thrust time is too transient, which will surely have influences on the guidance effect (see Section 5.1). In this work, a simplified (but practical enough) type of the thrust model [26] is used, as shown in Fig. 1.

Relations between the time-related quantities are given by

$$\Delta t_1=(10/9)t'_{90}+t_{id} \tag{4}$$

$$\Delta t_2=(10/9)t'_{10}+t_{sd} \tag{5}$$

where Δt_1 is thrust build-up time, Δt_2 the thrust tail-off time, t'_{90} the time from zero to 90% full thrust, t'_{10} the time from 100% to 10% full thrust, t_{id} the ignition delay, and t_{sd} the cutoff delay. Note that Δt_1 gives the minimum time required to reach the nominal thrust magnitude.

Fig. 1 shows the case in which the commanded thrust time (denoted by Δt_c) is sufficiently long and the nominal magnitude can be achieved. On the other hand, two cases will be incurred if the thrust time is too short, distinguished by comparing with t_{id} and Δt_1: (1) null thrust, if $\Delta t_c\le t_{id}$; (2) insufficient magnitude other than zero, if $t_{id}<\Delta t_c<\Delta t_1$. As for the latter case (shown in Fig. 2), we assume the thrust profile follows the same decreasing rate as the normal one shown in Fig. 1.

In conclusion, the thrust in the ignition and the cutoff phase (denoted by F_i and F_c), respectively, are expressed

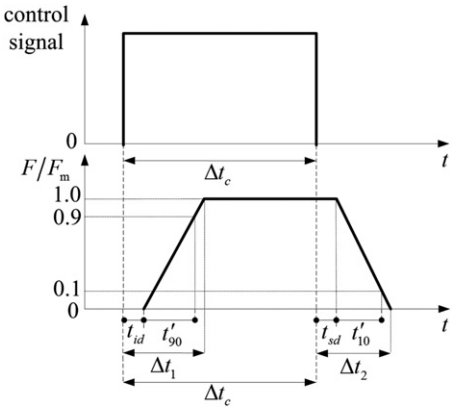

Fig. 1. A practical constant thrust model.

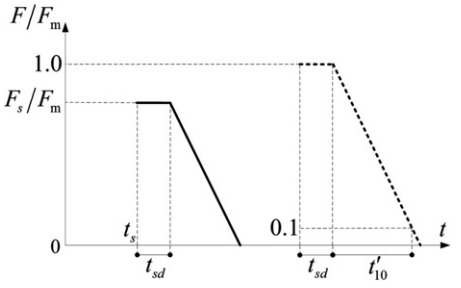

Fig. 2. Thrust profile in insufficient thrust time case.

as follows

$$F_i=\begin{cases}0 & \tau_1\le t_{id}\\ (0.9/t'_{90})(\tau_1-t_{id})F_m & t_{id}<\tau_1\le\Delta t_1\\ F_m & \tau_1>\Delta t_1\end{cases} \tag{6}$$

$$F_c=\begin{cases}F_s & \tau_2\le t_{sd}\\ F_s-(0.9/t'_{10})(\tau_2-t_{sd})F_m & t_{sd}<\tau_2\le t_r+t_{sd}\\ 0 & \tau_2>t_r+t_{sd}\end{cases} \tag{7}$$

where $\tau_1=t-t_i,\tau_2=t-t_s$, $t_r=(t'_{10}/0.9)(F_s/F_m)$, F_m the nominal thrust magnitude, and F_s the thrust when cutoff order is given.

4. Constant thrust time-fixed glideslope algorithm

Now we consider the time-fixed rendezvous problem. Assume that the chaser is located at an initial position $\boldsymbol{r}_0$ with an initial velocity $\boldsymbol{v}_0$ at time t_0. The problem is how to guide it to $\boldsymbol{r}_f^*$ with $\boldsymbol{v}_f^*$ within a given flight time T, where $\boldsymbol{r}_f^*$ is the chaser's desired final position (could be a desired parking node near the target or the target itself), and $\boldsymbol{v}_f^*$ the chaser's desired final velocity. The basic idea is to break down the trajectory into smaller arcs, which are to be implemented sequentially using the two-impulse transfer scheme [20] that, though highly idealized and unfit for a real flight, provides good insight for the glideslope guidance algorithm. Each individual arc is associated to an equally spaced guidance period (Δt), within which time the thruster fires along a fixed direction for a certain amount of time. To get a basic idea, see the sketch of the algorithm depicted in Fig. 3.

To be better elaborated, the whole algorithm is divided into three major components: the design of the time-fixed control parameters, the glideslope guidance procedure, and the implementation of the velocity increments. The first component deals with how to incorporate the flight time into the control law design; the second one gives the procedure to implement the rendezvous transfer using the parameters previously designed; the last one focuses on the practical thrusting issues when finite constant thrust is adopted.

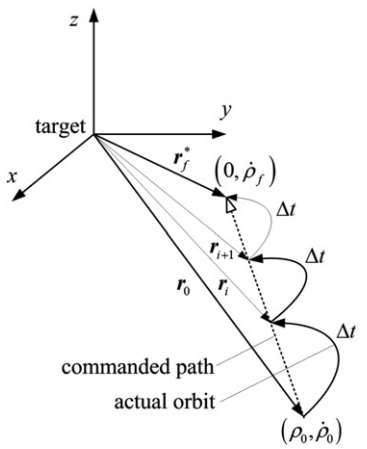

Fig. 3. Sketch of the glideslope algorithm.

4.1. Time-fixed control law design

Before giving the procedure of the algorithm, we first would like to present the design of the control parameters that are to be used in the algorithm. Define the vector from $\boldsymbol{r}_0$ to $\boldsymbol{r}_f^*$ as the commanded path $\boldsymbol{\rho}$, then we require the expected location at time t equal to

$$\boldsymbol{r}=\boldsymbol{r}_f^*-\rho\hat{\boldsymbol{\rho}} \tag{8}$$

where $\hat{\boldsymbol{\rho}}=\boldsymbol{\rho}/\|\boldsymbol{\rho}\|$, and ρ is the distance-to-go along $\boldsymbol{\rho}$, whose time derivative is about to be designed. It is demanded, out of safety consideration in RVD mission, that as ρ diminishes, the speed $\dot\rho$ must diminish with it. Suppose the boundary values of ρ_0, $\dot\rho_0$ and $\dot\rho_f$ are given

$$\begin{aligned}&\rho_0=\rho(t_0)=\|\boldsymbol{r}_f^*-\boldsymbol{r}_0\|\\ &\dot\rho_0=\dot\rho(t_0)<0\\ &\dot\rho_f=\dot\rho(t_f)<0\end{aligned} \tag{9}$$

where $\dot\rho_0<\dot\rho_f$ according to the safety requirement, and ρ_0 is the rendezvous distance. Different relationship between ρ and $\dot\rho$ can be postulated. The simplest one is the linear function, given by

$$\dot\rho=k\rho+b \tag{10}$$

From Eqs. (9) and (10), the time explicit expression for ρ and T are obtained as

$$\rho=(\rho_0+b/k)\exp(kt)-b/k \tag{11}$$

$$T=\ln(\dot\rho_f/\dot\rho_0)/k \tag{12}$$

where

$$k=\dot\rho_0-\dot\rho_f/\rho_0<0 \tag{13}$$

$$b=\dot\rho_f<0 \tag{14}$$

Seen from Eqs. (11) and (12), both ρ and T are functions of ρ_0 (a known parameter), $\dot\rho_0$ and $\dot\rho_f$, which reasonably makes them to be the key design parameters of our interest.

Unfortunately, there are no explicit expressions in which $\dot\rho_0$(or $\dot\rho_f$) can be expressed by T, which means one cannot directly solve the values of $\dot\rho_0$ and $\dot\rho_f$ out of a given T. We need more meaningful parameters to bridge a fixed time of flight. Note that the total number of arcs (denoted by N) is a critical parameter in the sense that it is associated with the number of thruster firings, thus having an impact on both the energy cost and guidance accuracy. We also notice that the ρ value of the final arc (final distance-to-go, denoted by ρ^*) also plays an important role in the control performance. By introducing these two parameters, both with clear physical meanings, we present an algorithm that is capable of solving for $\dot\rho_0$ and $\dot\rho_f$ with a given rendezvous distance ρ_0 and the flight time T, such that the whole guidance law can be established in a complete way. For clarity, we put it in the form of a proposition, and give the deduction in the appendix.

Proposition 1. Assume ρ_0, T, N, and ρ^* are given, and $\dot{\rho}_0$ and $\dot{\rho}_f$ are to be solved. Let

$$\gamma = \rho^*/\rho_0 \tag{15}$$

$$\eta = \dot{\rho}_f/\dot{\rho}_0 \tag{16}$$

If $\gamma \in (0,1/N)$ is satisfied, then we have

$$\dot{\rho}_0 = \rho_0 \ln(\eta)/[T(1-\eta)] \tag{17}$$

$$\dot{\rho}_f = \eta \dot{\rho}_0 \tag{18}$$

where η is the solution of

$$\eta^{(N-1)/N} = \gamma + \eta(1-\gamma) \tag{19}$$

See the appendix for detailed demonstration.

Note that η is a fixed unknown in Eq. (19), and has to be solved numerically with additional efforts (for instance, by Newton method). We use

$$\eta_0 = \left[\frac{N-1}{N(1-\gamma)}\right]^N \tag{20}$$

as its initial guess (see appendix Eq. (A5)), which enables a fast convergency process.

To sum up, by introducing η, variables $\dot{\rho}_0$ and $\dot{\rho}_f$ can now be explicitly related to a given T. Therefore, independent design parameters are now T, N, ρ_0 and ρ^*, based on which the analysis of the control effects will be done (see Section 5).

4.2. Procedure of the glideslope guidance algorithm

Once all the parameters in the algorithm have been designed, we can start the procedure of the guidance process. Although for brevity, only one guidance period is discussed, the subscript index (i) appearing in the equations will help to generalize the description of the whole process.

For a certain arc along the path, the i-th (index of the thruster firing, $i=1,\ldots,N+1$) control occurs at $\rho(t_{i-1})$ when $t_{i-1}=(i-1)\Delta t$ where $\Delta t=T/N$ is the guidance period, and pushes the chaser towards $\rho(t_i)$. From Eqs. (8) and (11), the corresponding positions are given by

$$\boldsymbol{r}_{i-1} = \boldsymbol{r}_f^* - [(\rho_0 + b/k)\exp(kt_{i-1}) - b/k]\hat{\boldsymbol{\rho}} \tag{22}$$

$$\boldsymbol{r}_i = \boldsymbol{r}_{i-1} + \gamma \exp(kt_{i-1})\hat{\boldsymbol{\rho}} \tag{23}$$

where $\gamma = (\rho_0 + b/k)[1-\exp(k\Delta t)]$ is a constant value. From Eq. (3), we have

$$\boldsymbol{r}_i = \boldsymbol{\Phi}_{11}\boldsymbol{r}_{i-1} + \boldsymbol{\Phi}_{12}\boldsymbol{v}_{i-1}^+ \tag{24}$$

$$\boldsymbol{v}_i^- = \boldsymbol{\Phi}_{21}\boldsymbol{r}_{i-1} + \boldsymbol{\Phi}_{22}\boldsymbol{v}_{i-1}^+ \tag{25}$$

where $\boldsymbol{v}_{i-1}^+$ represents the required velocity at r_{i-1} (navigational position), $\boldsymbol{v}_i^-$ the arrival velocity at r_i, and $\boldsymbol{\Phi}_{mn}, m,n=1,2$ the four 3×3 submatrices of the State Transition Matrix (STM) $\boldsymbol{\Phi}(t_i,t_{i-1})$, which is the solution of the following matrix Eq. (26)

$$\begin{cases} \dot{\boldsymbol{\Phi}}(t_i,t_{i-1}) = \mathbf{A}(t_{i-1})\boldsymbol{\Phi}(t_i,t_{i-1}) \\ \boldsymbol{\Phi}(t_{i-1},t_{i-1}) = \mathbf{I}_6. \end{cases} \tag{26}$$

Note that this matrix equation has to be numerically solved with the dynamics of the target due to the time variation property of $\boldsymbol{A}$.

From Eq. (24), we have the required velocity

$$\boldsymbol{v}_{i-1}^+ = \boldsymbol{\Phi}_{12}^{-1}(\boldsymbol{r}_i - \boldsymbol{\Phi}_{11}\boldsymbol{r}_{i-1}) \tag{27}$$

and then the velocity increment at r_{i-1}

$$\Delta\boldsymbol{v}_{i-1} = \boldsymbol{v}_{i-1}^+ - \boldsymbol{v}_{i-1}^- \tag{28}$$

where $\boldsymbol{v}_{i-1}^-$ is the chaser's arrival velocity given by the navigation system where the navigational error is introduced.

Note that $\Delta\boldsymbol{v}_{i-1}$ cannot be implemented by a finite constant thrust engine. Suitable transcription of this velocity increment is required (see Section 4.3), after which, the states of both spacecraft are numerically propagated using the full Solar System ephemeris until the next guidance period is initialized.

Special attention should be paid to the final corrective velocity increment, which is given by

$$\Delta\boldsymbol{v}_{N+1} = \boldsymbol{v}_f^* - \boldsymbol{v}_{N+1}^- \tag{29}$$

It was omitted in Ref. [23], but based on the results obtained in Sections 5.1 and 5.2, we consider it indispensable for diminishing the final velocity difference. Note that $\boldsymbol{v}_{N+1}^-$ is not the navigational velocity but the one predicted from Eq. (25). This is because, for the final velocity correction, the thruster should work before reaching the final time, and only if the value of $\Delta\boldsymbol{v}_{N+1}$ is given can the thrust time be determined (see next section). Recall that ρ is decreasing as time goes by, therefore, the accuracy of the predicted arrival velocity from Eq. (25) is growing, making Eq. (29) a good approximation.

4.3. Implementation of velocity increment

In the context of the finite constant thrust, since the magnitude of the thrust is known and constant (almost, such as the thrust model we use), the instantaneous $\Delta\boldsymbol{v}_i$ is transcribed to two other practical variables: the thrust time, and the direction.

For simplicity, the thrust time (denoted by Δt_c^i, $i=1,\ldots,N+1$) can be approximated using the norm of $\Delta\boldsymbol{v}_i$. Combining Tsiolkovsky equation [24] and Eq. (2), we obtain an approximation of the thrust time

$$\Delta t_c^i = mc[1-\exp(-\Delta V_i/c)]/F_m \tag{30}$$

where $\Delta V_i = \|\Delta\boldsymbol{v}_i\|$.

Associated with the thrust time, the turn-on time of the thruster should also be viewed. Liu [9] used a 1/2-time-ahead scheme, which requires the prediction of the arrival velocity. In this study, an on-site scheme is used, which means the thruster will not work until the thrust time is given by the guidance system based on measurements of the real-time state. In the last guidance period, however, the engine should be ignited Δt_c^N ahead in order to correct the final velocity difference.

Another concern is the thrust direction. We simply hold the thrust vector, throughout the entire thrust time, to be aligned with the direction of the velocity increment, i.e., $\boldsymbol{n}_i = \Delta\boldsymbol{v}_i/\Delta V_i$. Errors exist in holding this direction (due

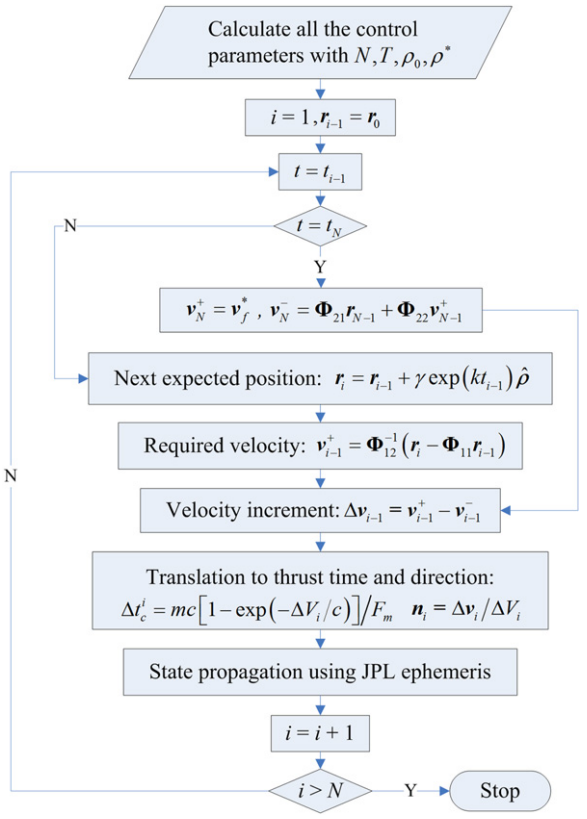

Fig. 4. The flowchart of the glideslope guidance procedure.

to attitude control errors and/or thruster installation errors) and should be taken into account (see Section 5.2).

For clarity, we give a flowchart (see Fig. 4) of the glideslope guidance procedure as a conclusion of this section.

5. Numerical results

Simulation is done using the JPL DE405 ephemeris, taking into account all the gravitational forces from Earth, Moon, Sun and other planets. The epoch is arbitrarily selected to be 56279.32388311 MJD (18 Dec 2012 07:46:23.500 UTCG). A location on a quasi-periodic halo orbit (8000 km of z-amplitude, in the real Earth–Moon system) is employed as the initial target's position, as shown in Fig. 5. The chaser's properties are listed in Table 1, where all the thrust-related values are normal to the current engine technology. Without losing generality, the initial and final relative states of the chaser, not necessarily on a halo orbit, are given in Table 2, where D ($D=\rho_0$ since $y=z=0$) is the rendezvous distance (the tested range is 100–2000 km in this work, coherent to the one covered by the typical near-range guided phase in RVD).

Using the proposed algorithm, any parameter tetrad (T,N,ρ^*,D) would give a rendezvous orbit. To assess the control performance, four indices are surveyed, which are the final position error, the final velocity error, total velocity increments, and mass consumption, defined as follows,

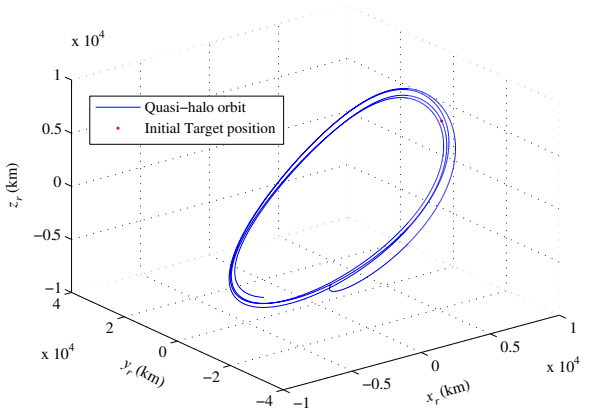

Fig. 5. Quasi-halo orbit in full ephemeris model (Earth–Moon rotating frame).

Table 1
Chaser properties.

Parameter	Value
m_0 (kg)	3000
F_m (N)	1000
c (m/s)	2800
t_{id} (s)	0.002
t_{sd} (s)	0.002
t'_{90} (s)	0.010
t'_{10} (s)	0.008

Table 2
Boundary conditions.

Component	At initial time	At final time
x (m)	D+500.0	500.0
y (m)	0.0	0.0
z (m)	0.0	0.0
v_x (m/s)	−10.0	−1.0
v_y (m/s)	5.0	0.0
v_z (m/s)	3.0	0.0

respectively

$$\|\Delta\boldsymbol{r}_f\| = \|\boldsymbol{r}_f - \boldsymbol{r}_f^*\| \tag{31}$$

$$\|\Delta\boldsymbol{v}_f\| = \|\boldsymbol{v}_f - \boldsymbol{v}_f^*\| \tag{32}$$

$$\Delta V = \sum_i \Delta V_i \tag{33}$$

$$\Delta m = m_f - m_0 \tag{34}$$

where $\boldsymbol{v}_f$ is the actual final velocity of the chaser, m_0 the initial mass, m_f the final mass.

5.1. Standard trajectory case

In the standard trajectory case, no error is considered. The objective is to validate the feasibility of the proposed guidance algorithm.

First, we investigate the impact of D and T, which are closely related to a specified mission. As a matter of fact, the shorter the flight time (usually the more preferable in RVD) is, the more difficult it will be for the rendezvous control. In view of the possible time-rigorous missions, such as the crew retreat from a space station in emergency, the flight time we consider in this paper will be between 3–12 h (flight time less than 3 h tends to give very unfavorable performance for most cases in our tests). Arbitrarily set $N=5$ and $\rho^*=50$ m. The surfaces in Fig. 6 show the control performance with different $D-T$ combinations, whereon the points mark the calculated cases. As can be seen, for a specific D (in km), different T will result in distinct final position errors ($\|\Delta \boldsymbol{r}_f\|$ values), some of which even reach the magnitude of 10 km, while some are less than 1 m. Very large $\|\Delta \boldsymbol{r}_f\|$ occurs only when T is comparatively short, which means an over-rigid requirement of flight time will exceed the thruster's ability. As expected, the best choice of T, which produces the smallest $\|\Delta \boldsymbol{r}_f\|$, grows as D increases. A similar situation happens to $\|\Delta \boldsymbol{v}_f\|$, and in all cases it lays below 4 mm/s, which is more than sufficient for a real mission. As for ΔV and Δm, they both decreases smoothly as T increases within its range. This fact indicates that the control accuracy and the energy cost cannot be satisfied most at the same time. A compromise between guidance accuracy and energy cost has to be made in determining a proper T for a given D.

Note that three unexpected points appear in the upper two subplots in Fig. 6, whose $\|\Delta \boldsymbol{r}_f\|$ values have shown abrupt rises. The one with $D=1200$ km and $T=10$ h is sorted out for a close inspection. Fig. 7 shows the detail of this instance, in which the orbit in RVD frame is plotted in Fig. 7a and b, the orbit in rotating frame in Fig. 7c, and the thrust and mass profiles in Fig. 7d. Thicker lines indicate thrusting arcs (Fig. 7a–c), while the circle and the points (Fig. 7a and b) signify $\boldsymbol{r}_f^*$ and the expected locations along ρ, respectively. One can see in Fig. 7b, the last but one control (where there is an inflection) is unable to draw the orbit towards the destination, thus a relatively large $\|\Delta \boldsymbol{r}_f\|$ has been produced. Checking the thrust history, we know the reason lies in that the corresponding burn time ($\Delta t_{N-1}=0.0112$ s) is too short to reach the nominal thrust magnitude, as shown in Fig. 7d (at $t=8$ h). Similar occasions happened to the other two cases. Therefore, we can conclude that the insufficient implementation of $\Delta \boldsymbol{v}_i$ will largely hazard the position accuracy, and should be paid special attention to in the finite thrust guidance applications.

Next, consider the influence of N–T combinations on the control performance. Calculations are done with respect to typical values of $D=500$ km and $\rho^*=50$ m. Note that N is discrete integers. Results are given in Fig. 8. In all the four subplots, curves tend to gather as N increases, implying too many thruster firings are unnecessary for achieving certain performance. $\|\Delta \boldsymbol{r}_f\|$ varies greatly in magnitude, and its minimum happens at $N=5$, $T=5$ h. Though varying abruptly for some N as well, $\|\Delta \boldsymbol{v}_f\|$ is kept under good control (all below 1 mm/s, and curves for $N>6$ are hardly discernable). In contrast, ΔV and Δm change much regularly with N and T. They decrease as T increases, and behave reversely with respect to N, which means too short a flight time or too many thruster firings will induce larger energy cost.

Last, check the impact of ρ^* selections. Other three parameters are chosen to be $D=500$ km, $T=5$ h, and $N=5$.

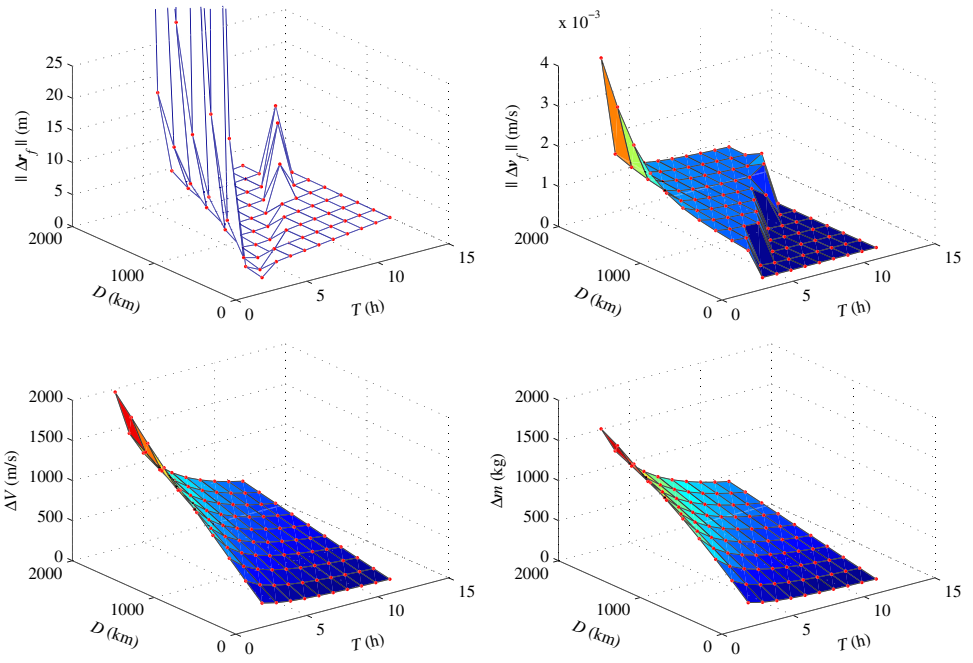

Fig. 6. Control effects with different D–T combinations ($N=5$ and $\rho^*=50$ m).

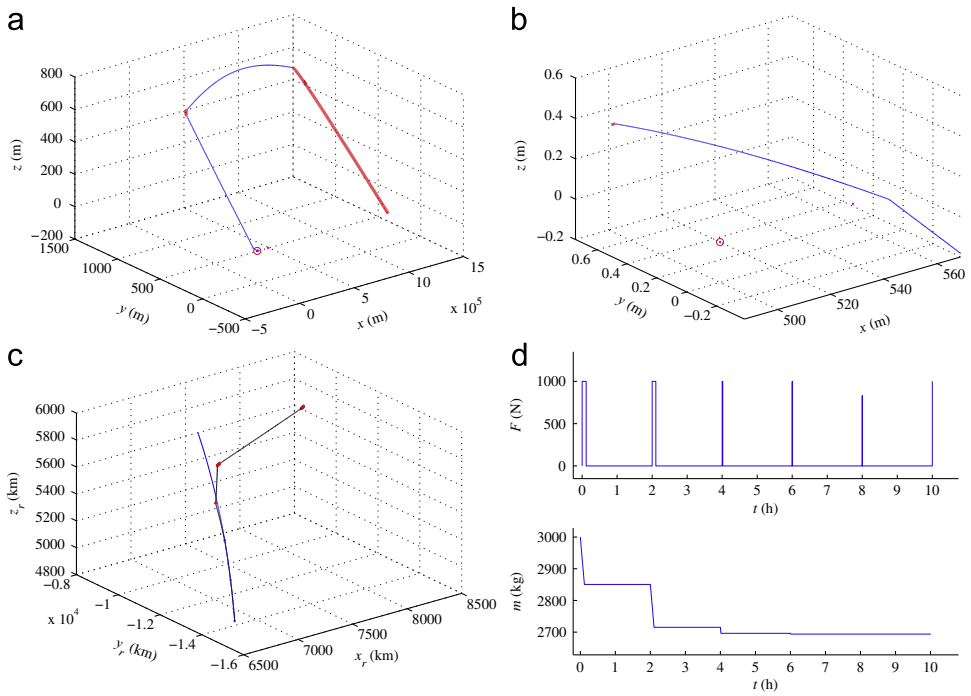

Fig. 7. Impact of insufficient delta-v implementation (D=1200 km, T=10 h, N=5, and ρ^*=50 m). (a) Full orbit in RVD frame, (b) close-up of the last arc, (c) full orbit in rotating frame, and (d) thrust and mass history.

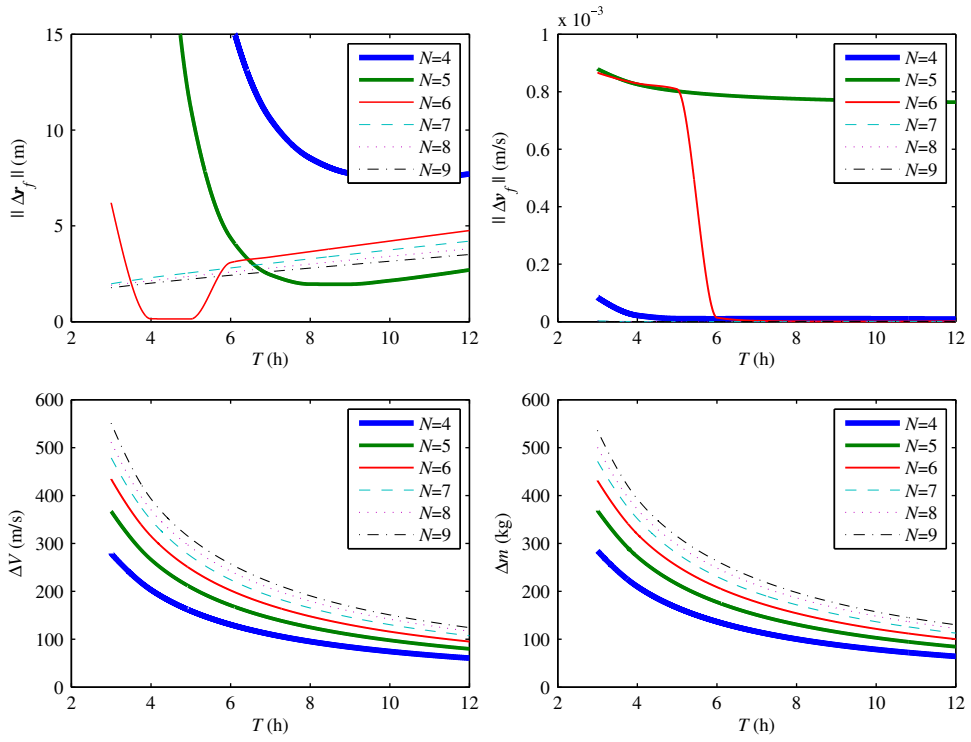

Fig. 8. Control effects of different N–T combinations (D=500 km and ρ^*=50 m).

Results are given in Fig. 9, where points on the lines represent the calculated instances. One can see that $\|\Delta \boldsymbol{r}_f\|$ shows a rising trend as ρ^* grows, with the exception at ρ^*=100 m where, as expected, an insufficient delta-v implementation occurs. ΔV and Δm both decrease as ρ^* increases, and around 100 m/s of delta-v difference exists

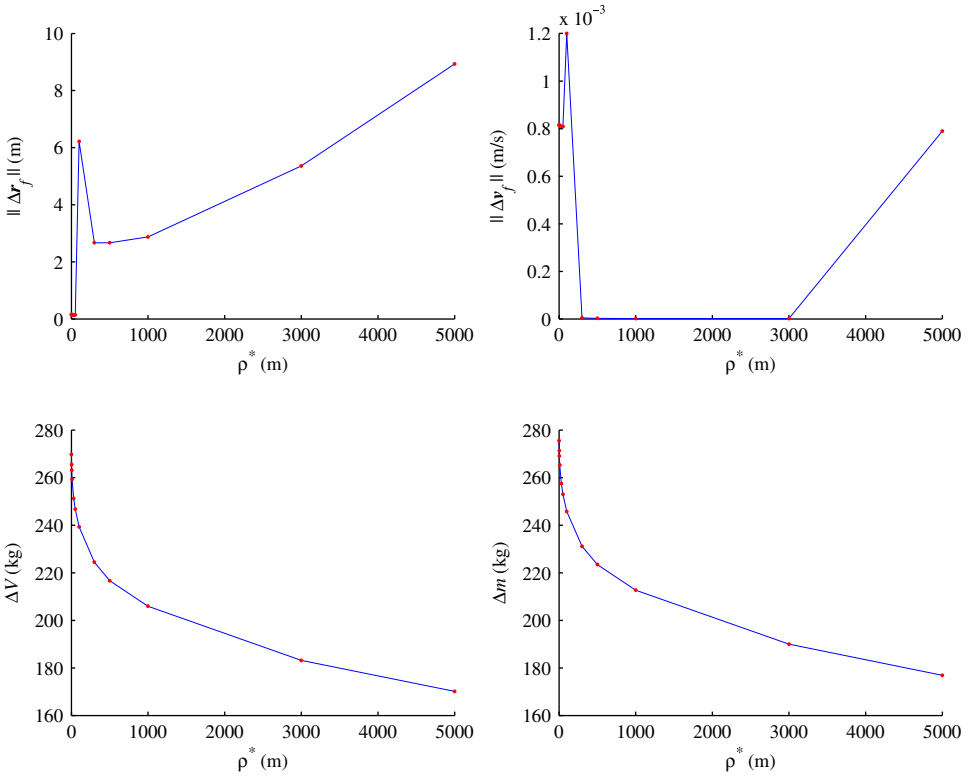

Fig. 9. Impact of ρ^* selections (D=500 km, T=5 h, and N=5).

for a 5 km range of ρ^*, which indicates that ρ^* has a great impact on the energy cost.

To sum up this subsection, a large number of tests, which are grouped by the independent design parameters, have validated the proposed algorithm's feasibility. Each parameter in the set (T, N, ρ^*, D) plays a different role in affecting the overall control performance. Although optimization is not the subject of this work, we can still conclude that Multi-Objective Optimization (MOO) method should be adopted to get the best combination (in fact, there will be many since the Pareto frontier is a solution set) of these parameters when both the guidance accuracy and energy cost are considered.

5.2. Monte Carlo analysis

This subsection deals with the robustness of the proposed algorithm. In real applications, there are various errors existing and the orbit will, inevitably, deviate from its standard path (the designed one). We are interested in the performance of the algorithm when errors are introduced. Navigation error and control error are the main concerns in this study.

Navigation error, including the position error and the velocity error, comes from the navigational equipment and methods, which is assumed to be in regard with the distance between chaser and $\boldsymbol{r}_f^*$ (denoted by R, varying with time) in this analysis. In addition, thrust direction error, resulting from attitude control error or thruster mounting error, is also considered. Both errors are assumed to be normally distributed with zero means, and the standard deviations are given in Table 3, where σ_{p_j} is the standard deviation of navigational position error, σ_{v_j} the standard deviation of navigational velocity error, $\sigma_{\Delta \boldsymbol{v}_j}$ the standard deviation of thrust direction error, and j=x,y,z.

Table 3
Error distributions.

Standard deviation	$R \le 2$ km	$R > 2$ km
$\sigma_{\boldsymbol{p}_j}$ (m)	0.1	1
$\sigma_{\boldsymbol{v}_j}$ (m/s)	0.001	0.01
$\sigma_{\Delta \boldsymbol{v}_j}$	0.5%	–

Monte Carlo analyses based on 300 trials are conducted, with respect to three cases that consider only the navigational error, only the thrust direction error, and the both, respectively. The baseline standard trajectory is taken from Fig. 6, with D=500 km, T=5 h, N=5, and ρ^*=50 m. Results are given in Table 4 and Fig. 10. In Table 4, statistics of $\|\Delta \boldsymbol{r}_f\|$, $\|\Delta \boldsymbol{v}_f\|$, ΔV and Δm in the three cases are listed: the mean, the standard deviation, the maximum, and the minimum of the 300 trials. Values of the standard orbit are also given. Fig. 10 shows the statistical distribution of the third case in which both errors are considered.

It is apparent in Table 4 that the navigation error accounts for most part of the deviations. $\|\Delta \boldsymbol{r}_f\|$ is largely

Table 4
Monte Carlo simulation results (300 trials).

Case	Statistics	$\|\Delta \boldsymbol{r}_f\|$ (m)	$\|\Delta \boldsymbol{v}_f\|$ (m/s)	ΔV (m/s)	Δm (kg)
Standard orbit	–	0.141	8.088e−4	246.707	253.016
Navigational error only	Average	5.745	0.002	246.710	253.019
	Std. deviation	2.507	7.365e−4	0.036	0.035
	Maximum	13.041	0.004	246.814	253.121
	Minimum	0.537	2.616e−4	246.619	252.929
Thrust direction error only	Average	0.163	8.090e−4	246.711	253.020
	Std. deviation	0.040	1.005e−6	0.003	0.003
	Maximum	0.455	8.181e−4	246.719	253.028
	Minimum	0.133	8.065e−4	246.701	253.010
Both errors	Average	5.703	0.002	246.709	253.018
	Std. deviation	2.604	7.916e−4	0.035	0.035
	Maximum	14.258	0.005	246.817	253.124
	Minimum	0.564	6.244e−5	246.619	252.930

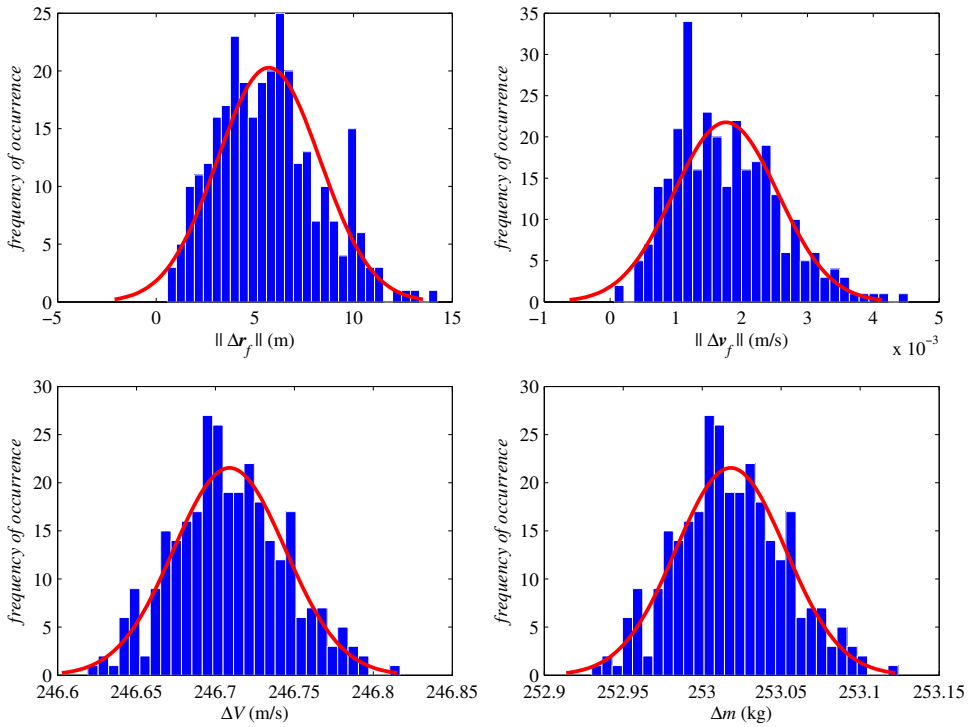

Fig. 10. Statistical distribution of control effect indices with both errors considered.

affected by the introduced errors, with the maximum value near 15 m, while the minimum around 0.6 m when both errors are considered. In contrast, $\|\Delta \boldsymbol{v}_f\|$, ΔV, and Δm are only slightly influenced by the errors. $\|\Delta \boldsymbol{v}_f\|$ is always under 5 mm/s, and the maximum deviations of ΔV and Δm are also less than 0.1 m/s and 0.1 kg, respectively.

Therefore, it can be concluded that the last firing of the algorithm has very satisfactory corrective effect on the final relative velocity, but not likely on the position. In contrast, the control prior to the last one is very essential for the final position accuracy. We should also notice that, although decreased as compared with the standard case, the guidance accuracy is still sufficient for initializing a final approach phase that will finally guide the chaser to dock with the target.

6. Conclusions

The proposed constant-thrust glideslope algorithm provides an effective approach to guide the spacecraft to rendezvous with a target in multi-body realm. It is remarkable that a new strategy for designing parameters with the fixed-time constraint is presented, which will benefit missions that are time-sensitive. Simulations indicate that the final position accuracy should be the primary concern, which tends to be easily affected by

insufficient implementation of the delta-v. With common errors in consideration, the method can reach an average control accuracy of less than 6 m and 2 mm/s (for a rendezvous range of 500 km) for the final position and velocity, respectively, making it a good candidate for the near-range guided phase in halo orbit rendezvous.

Moreover, the core of the method is quite general. It applies not only to the approaching operation in a rendezvous mission, but retreating or fly-around movements as well. The differences lie in the characteristics of the target only. Moreover, the dynamics involved in the algorithm add no constraints on either the type of the orbits or the scope of the three body system. For instance, it can be employed to implement the Lissajous orbit rendezvous in the Sun–Earth/Moon system.

Acknowledgments

This work was supported by the National Natural Science Foundation of China (Grants No. 10702078 and 10973048).

Appendix A. Demonstration of Proposition 1

From the definition of ρ^*, we have

$$\rho^* = \rho(t_{N-1}) \tag{A1}$$

Using Eqs. (11) and (A1),

$$(\rho_0 + b/k)\exp[(N-1)kT/N] - b/k = \rho^* \tag{A2}$$

Substituting Eqs. (12), (15) and (16) into Eq. (A2) yields

$$\eta^{(N-1)/N} = \gamma + \eta(1-\gamma)$$

which is Eq. (19), where $\eta,\gamma \in (0,1)$ by their definitions.

Now analyze the solutions of Eq. (19). Set

$$f(\eta) = \eta^{(N-1)/N} - \eta(1-\gamma) - \gamma \tag{A3}$$

where $\eta,\gamma \in (0,1)$. Note that if $\eta \to 0, f \to -\gamma < 0$, and if $\eta \to 1$, $f \to 0$, thus one solution of Eq. (A3) can be insured only if

$$f(\tilde{\eta}) > 0 \tag{A4}$$

where $\tilde{\eta}$ gives the maximum of $f(\eta)$.

Differentiating Eq. (A3) and setting $f'(\eta)=0$, we have

$$\tilde{\eta} = \left[\frac{N-1}{N(1-\gamma)}\right]^N \tag{A5}$$

Recall that $\tilde{\eta} \in (0,1)$. Thus, a strengthened constraint on γ is solved as

$$0 < \gamma < 1/N \tag{A6}$$

Substituting Eq. (A5) into Eq. (A4) yields

$$\gamma(1-\gamma)^{N-1} < (N-1)^{N-1}/N^N \tag{A7}$$

Now check the inequality of Eq. (A7). Set

$$g(\gamma) = \gamma(1-\gamma)^{N-1} - (N-1)^{N-1}/N^N \tag{A8}$$

and $g(\gamma) < 0$ is required. From Eqs. (A6) and (A8), we see that if $\gamma \to 0$,

$$g(\gamma) \to -(N-1)^{N-1}/N^N < 0$$

and if $\gamma \to 1/N$, $g(\gamma) \to -0$. In addition, for $\forall \gamma \in (0,1/N)$,

$$g'(\gamma) = (1-N\gamma)(1-\gamma)^{N-2} > 0$$

Now we can safely draw the conclusion that Eq. (19) will always have only one solution if $\gamma \in (0,1/N)$ is satisfied.

From Eqs. (12), (15), and (16), we have

$$T = \rho_0 \ln(\eta)/[\dot{\rho}_0(1-\eta)] \tag{A9}$$

Then, from Eqs. (A9) and (16), $\dot{\rho}_0$ and $\dot{\rho}_f$ are given by

$$\dot{\rho}_0 = \rho_0 \ln(\eta)/[T(1-\eta)]$$

$$\dot{\rho}_f = \eta\dot{\rho}_0$$

which are Eqs. (17) and (18), respectively.

References

[1] W.H. Clohessy, R.S. Witshire, Terminal guidance system for satellite rendezvous, J. Aerosp. Sci. 27 (9) (1960) 653–658,674.
[2] J.E. Prussing, Optimal four-impulse fixed-time rendezvous in the vicinity of a circular orbit, AIAA J. 7 (5) (1969) 928–935.
[3] J.E. Prussing, Optimal two- and three-impulse fixed-time rendezvous in the vicinity of a circular orbit, AIAA J. 8 (7) (1970) 1221–1228.
[4] J.B. Jones, Optimal rendezvous in the neighborhood of a circular orbit, J. Astronaut. Sci. 24 (1) (1976) 55–90.
[5] T.E. Carter, J. Brient, Linearized impulsive rendezvous problem, J. Optim. Theory Appl. 86 (3) (1995) 553–584.
[6] J.E. Prussing, Optimal impulsive linear systems: sufficient conditions and maximum number of impulses, J. Astronaut. Sci. 43 (2) (1995) 195–206.
[7] W. Fehse, Automated Rendezvous and Docking of Spacecraft, Cambridge University Press, London, 2003.
[8] J.L. Goodman, History of space shuttle rendezvous and proximity operations, J. Spacecraft Rockets 43 (5) (2006) 944–959.
[9] L. H. Liu. Research on Autonomous Rendezvous Guidance and Control for Spacecraft (in Chinese), Ph.D. Dissertation, National University of Defense Technology, Changsha, 2007.
[10] M. Lo, S. Ross, The Lunar L1 Gateway: Portal to the Stars and Beyond, in: Paper AIAA 2001-4768, AIAA Space 2001 Conference and Exposition, Albuquerque, NM, August 28–30 2001.
[11] V. R. Bond, S. J. Sponaugle, M. F. Fraietta, and S. F. Everett, Cislunar Libration Point as a Transportation Node for Lunar Exploration, in: Paper AAS 91-193, AAS/AIAA Spaceflight Mechanics Meeting, Houston, TX, February 1991.
[12] G. Gómez, J. Masdemont, C. Simó, Quasi-halo orbits associated with libration points, J. Astronaut. Sci. 42 (2) (1998) 135–176.
[13] L.A. Hiday-Johnston, K.C. Howell, Transfers between Libration-point Orbits in the Elliptic Restricted Problem, in: Paper AAS 92–126, AIAA/AAS Space Flight Mechanics Meeting, Colorado, 1992.
[14] K.C. Howell, L.A. Hiday-Johnston, Time-free transfers between libration-point orbits in the elliptic restricted problem, Acta Astronaut. 32 (4) (1994) 245–254.
[15] L.A. Hiday-Johnston, K.C. Howell, Impulsive time-free transfers between halo orbits, Celestial Mech. Dyn. Astron. 64 (1996) 281–303.
[16] D.F. Lawden, Optimal Trajectories for Space Navigation, Butterworths, London, 1963.
[17] G. Gómez, A. Jorba, C. Simó, Study of the transfer between halo orbits, Acta Astronaut. 43 (9–10) (1998) 493–520.
[18] C.E. Roberts, Sun–Earth L1 Region Halo-to-halo Orbit and Halo-to-Lissajous Orbit Transfers, in: 18th International Symposium on Space Flight Dynamics, Munich, Germany, 2004.
[19] M. Volle, Optimal Variable-specific-impulse Rendezvous Trajectories between Halo Orbits, in: Paper ISTS 2006-d-73, 19th International Symposium on Space Flight Dynamics, Kanazawa, Japan, 2006.
[20] B.L. Jones, A Guidance and Navigation System for Two Spacecraft Rendezvous in Translunar Halo Orbit, Ph.D. Dissertation, Department of Aerospace Engineering and Engineering Mechanics, The University of Texas at Austin, Austin, TX, May, 1993.
[21] A. Marinescu, A. Nicolae, M. Dumitrache, Optimal Low-Thrust Libration Points Rendez-vous in Earth–Moon System, in: AIAA Paper 99–4050, 1999.

[22] A. Marinescu, M. Dumitrache, The Nonlinear Problem of the Optimal Libration Points Rendezvous in Earth–Moon System, in: AIAA Paper 2000–4433, 2000.
[23] H.B. Hablani, M.L. Tapper, D.J. Dana-Bashian, Guidance and relative navigation for autonomous rendezvous in a circular orbit, J. Guid. Control Dynam. 25 (3) (2002) 553–562.
[24] B.A. Conway, Spacecraft Trajectory Optimization, Cambridge Aerospace Series, Cambridge, England, UK, 2010.
[25] R.J. Luquette, Nonlinear Control Design Techniques for Precision Formation Flying at Lagrange Points, Ph.D. Dissertation, Maryland University, College Park, 2006.
[26] H.Y. Zhao, Dynamics and Guidance of Reentry Vehicle (in Chinese), National University of Defense Technology, Changsha, 1997, pp. 439–442.